AFRL-SN-RS-TR-1998-113
In-House Report
May 1998

TIME-DOMAIN DECONVOLUTION REMOVES THE EFFECTS OF NEAR-FIELD SCATTERERS

Thomas M. Roberts

APPROVED FOR PUBLIC RELEASE; DISTRIBUTION UNLIMITED

**AIR FORCE RESEARCH LABORATORY
SENSORS DIRECTORATE
ROME RESEARCH SITE
ROME, NEW YORK**

19990413160

This report has been reviewed by the Air Force Research Laboratory, Information Directorate, Public Affairs Office (IFOIPA) and is releasable to the National Technical Information Service (NTIS). At NTIS it will be releasable to the general public, including foreign nations.

AFRL-SN-RS-TR-1998-113 has been reviewed and is approved for publication.

APPROVED:

THOMAS M. ROBERTS
Antennas Technology Branch
Electromagnetics Technology Division

FOR THE DIRECTOR:

ROBERT V. McGAHAN
Technical Director
Electromagnetics Technology Division

If your address has changed or if you wish to be removed from the Air Force Research Laboratory Rome Research Site mailing list, or if the addressee is no longer employed by your organization, please notify AFRL/SNHA, 31 Grenier St., Hanscom AFB MA 01731-3010. This will assist us in maintaining a current mailing list.

Do not return copies of this report unless contractual obligations or notices on a specific document require that it be returned.

ALTHOUGH THIS REPORT IS BEING PUBLISHED BY AFRL, THE RESEARCH WAS ACCOMPLISHED BY THE FORMER ROME LABORATORY AND, AS SUCH, APPROVAL SIGNATURES/TITLES REFLECT APPROPRIATE AUTHORITY FOR PUBLICATION AT THAT TIME.

REPORT DOCUMENTATION PAGE

1. AGENCY USE ONLY *(Leave blank)*	2. REPORT DATE	3. REPORT TYPE AND DATES COVERED
	May 1998	In-House

4. TITLE AND SUBTITLE

TIME-DOMAIN DECONVOLUTION REMOVES THE EFFECTS OF NEAR-FIELD SCATTERERS

5. FUNDING NUMBERS

PE - N/A
PR - 2304
TA - I3
WU- 02

6. AUTHOR(S)

Thomas M. Roberts

7. PERFORMING ORGANIZATION NAME(S) AND ADDRESS(ES)

Air Force Research Laboratory/SNHA
31 Grenier St.
Hanscom AFB, MA 01731-3010

8. PERFORMING ORGANIZATION REPORT NUMBER

AFRL-SN-RS-TR-1998-113

9. SPONSORING/MONITORING AGENCY NAME(S) AND ADDRESS(ES)

Air Force Research Laboratory/SNHA
31 Grenier St.
Hanscom AFB, MA 01731-3010

10. SPONSORING/MONITORING AGENCY REPORT NUMBER

AFRL-SN-RS-TR-1998-113

11. SUPPLEMENTARY NOTES

Air Force Research Laboratory Project Engineer: Thomas M. Roberts/SNHA, Hanscom AFB, MA/(617) 377-1362

12a. DISTRIBUTION AVAILABILITY STATEMENT

Approved for public release; distribution unlimited.

12b. DISTRIBUTION CODE

13. ABSTRACT *(Maximum 200 words)*

This paper studies a deconvolution problem that models the removal of interference caused by objects in the near field of antennas. Such interference affects antennas on complicated objects, such as ships and aircraft. Infinitely many time-domain deconvolution algorithms are considered here, of which the best one -- being stable and $O(h^2)$ accurate, and $O(h^4)$ accurate after Richardson extrapolation -- may compete with Fourier and Laplace methods. Special care is taken to find an algorithm that accommodates discontinuity-related numerical noise in finite-difference-time-domain data.

14. SUBJECT TERMS

antenna, interference, deconvolution, near-field, integral equation, time domain, pulse, FDTD, finite-difference

15. NUMBER OF PAGES

18

16. PRICE CODE

17. SECURITY CLASSIFICATION OF REPORT	18. SECURITY CLASSIFICATION OF THIS PAGE	19. SECURITY CLASSIFICATION OF ABSTRACT	20. LIMITATION OF ABSTRACT
UNCLASSIFIED	UNCLASSIFIED	UNCLASSIFIED	UL

CONTENTS

ILLUSTRATIONS

ACKNOWLEDGMENTS

Time-domain Deconvolution
Removes the Effects of
Near-field Scatterers

1. INTRODUCTION

This report studies the removal of interference caused, in linear propagation, by near-field scatterers. The report's numerical example is a schematic representative for the removal of electromagnetic interference caused by a mast, wing tip, or fin that is in the near field of a ship or airborne receiving antenna [1].

The above problem will be shown to reduce to the deconvolution of the right-hand side of Eq. (1) below, which could be easily accomplished using Fourier or Laplace transforms. This report's goal, therefore, is to find what may be the best alternative time-domain algorithm. The best time-domain algorithm considered here is competitive with frequency-domain algorithms in that the t-domain algorithm feeds one-degree-smoothed data into a first-kind-Volterra-equation solver [2] that is second-order accurate and stable, and for which Richardson extrapolation yields a fourth-order-accurate method. Special care is taken to find a deconvolution algorithm that accommodates discontinuity-related numerical noise in finite-difference-time-domain (FDTD) data.

The central equation for the preferred algorithm will be shown to be

$$\int_0^t R(s)\mathrm{d}s = \int_0^t K_\mathrm{H}(t-s)f_\mathrm{inc}(s)\mathrm{d}s, \tag{1}$$

where R is the received signal that results from the corruption of the incident signal f_inc by a near-field scatter. The identity Eq. (1) follows directly from the Duhamel theorem [3] concerning the Heaviside-step response K_H of a linear system. The discontinuous kernel K_H will be computed here using an FDTD (finite difference time domain) method, despite the noise introduced by the FDTD propagation of a discontinuity. Indeed, this approach Eq. (1) was stimulated by an earlier paper [4], which established the usefulness of FDTD propagation of discontinuities in linear scattering. This report and [4] are complementary in that the central operator in [4] is a convolution and the central operator here is the deconvolution of Eq. (1).


A prototype problem will be defined in Section 2. Section 3 considers an infinite sequence of time-domain algorithms, each of which could solve the prototype problem. The best of these algorithms is found using two numerical criteria. Section 4 solves the prototype problem of Section 2 numerically. The conclusion (Section 5) describes the relation of the present work to an earlier-published paper [4], which together find two uses for the FDTD propagation of discontinuous functions. The potential use of laboratory data also is discussed in Section 5. The Appendix studies the only approximation (truncation of superluminal components) that is made in the best time-domain algorithm.

2. A PROTOTYPE PROBLEM

A prototype problem is defined here, and it will later be solved numerically in Section 4 as an example of a more general procedure developed in Section 3. This prototype problem involves the realistic parameters of an existing antenna [5], which is sketched in Figure 1. This section defines the problem, says what it represents, and then explains how this report's analysis applies to more complicated problems that involve multiple scattering.
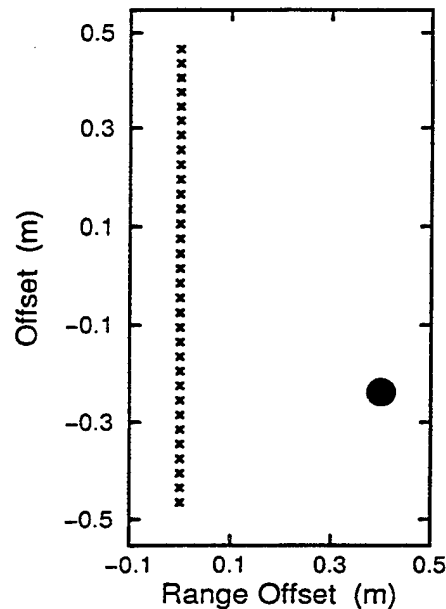
Figure 1. Scale drawing of a metal disk and the 32 locations ($\times$) where the total field is received inside the computational domain.

There is initially, for $t < 0$, no field in the rectangular domain in Figure 1. At $t = 0$ a t-dependent field becomes incident uniformly from the right, with its electric-field component being always perpendicular to the page. This field represents a pulse that is incident from a distant source, known also as a soft

source, and the incident pulse is therefore added, at each timestep, to the total field at each point on the right-hand edge of Figure 1. The incident field itself is never received; instead, it propagates through free space ($\varepsilon = 1$) and scatters from a conducting ($\sigma \leq \infty$) object, which is drawn as a disk in Figure 1, and the total t-dependent electric field is then measured at each cross-marked location in the figure. It is assumed that the measurements do not perturb the field. Let $R_j(t)$ be the field that is measured at the jth location. Then this report's prototype problem is as follows: Given the total field $R_j(t)$ at a single known location, knowing that the field was produced by a soft-source plane-wave pulse incident from a known direction, and knowing also the location, shape, and composition (ε and σ) of the scatterer, one must then compute the time trace of the incident pulse.

The prototype problem (above) is a schematic representative for the removal of electromagnetic interference with a ship or airborne antenna that is in the near field of a mast, wing tip, or fin [1]. In Section 4 the incident field will be taken to be a 1-cycle sinusoid with a 5.45-GHz carrier frequency, whose free-space wavelength is approximately the diameter of the steel disk in Figure 1. Because the wavelength is also comparable to the length of two cross-marked intervals in Figure 1, this prototype problem represents a 32-element phased-array radar antenna [5] that has a wavelength-sized metal pipe located 40-cm in front of it. That pipe introduces a reasonably large amount of interference, which we seek to remove.

One of the prototype problem's more idealized assumptions is that the antenna measures the field nonperturbatively. This assumption neglects the important practical effect of multiple scattering among the 32 elements, and it thereby conforms to the tradition that prototype problems be simple. One way to simulate multiple scattering, however, would be to have an imperfect absorber in a small area near each ×-marked element, and perhaps to have a small conductor behind each imperfect absorber. In any case, the FDTD response would still be a linear operator with respect to the incident field, regardless of what reasonable conductors and absorbers are used. The analysis in this report would apply without change to any such reasonable linear system, including all linear systems that have multiple scattering.

3. NUMERICAL METHODS AND THEIR PROPERTIES

Because the deconvolution problem (Section 2) involves a linear system, it can be easily solved using Fourier or Laplace transforms. This section will consider infinitely many time-domain alternatives (Eqs. (2)) and will use two numerical criteria to select the best alternative.

Linearity yields infinitely many integral equations for the incident field f_{inc}. The equations are

$$R(t) = \int_0^t K_\delta(t-s) f_{inc}(s) ds \qquad (2a)$$

$$\partial_t^{-1} R(t) = \int_0^t K_H(t-s) f_{inc}(s) ds \qquad (2b)$$

$$\partial_t^{-2} R(t) = \int_0^t K_{tH}(t-s) f_{inc}(s) ds, \qquad (2c)$$

$$\vdots \qquad\qquad\qquad \vdots$$

where ∂_t^{-2} is the square of the antiderivative operator $\partial_t^{-1} R(t) \equiv \int_0^t R(s) ds$, and where the subscripted kernels indicate the delta-function response, K_δ, the Heaviside response, K_H, and the ramp-function $[tH(t)]$ response, K_{tH}, at the location where the received signal R is measured. In linear hyperbolic systems, such as linear t-domain electromagnetics, a propagation-of-singularities argument [3] shows that K_δ has a nonzero delta-function component; however, [4] showed that a bounded (L_∞) approximation to δ could be propagated usefully using FDTD. Assuming that K_δ in Eq. (2a) would be computed using such an L_∞ computation, it follows that the sequence of Eqs. (2a), (2b), (2c), ... are all first-kind Volterra integral equations (for f_{inc}) with convolution kernels; whence the word "deconvolution" was brought into the title of this report.

We now consider a numerical property that will be used as a selection criterion for Eqs. (2): Linz [2] showed that if the left-hand side of a general first-kind Volterra equation

$$L(t) = \int_0^t K(t,s) f(s) ds \qquad (3)$$

is perturbed by an amount ΔL then the resulting perturbation in the solution of Eq. (3) is, in what is probably the best case,

$$\Delta f = O\left(h^{-1} \Delta L\right). \qquad (4)$$

4

That ill-posedness result in Eq. (4) favors equations that have smooth left-hand sides; consequently, Eq. (2a) is eliminated as a candidate.

We still have infinitely many candidates — Eqs. (2b), (2c), ... — from which we will be able to extract the best candidate only after a method for solving first-kind equations is described. This method will be described as it applies to the eventually preferred candidate Eq. (2b), but the same method is easily adapted to suit all candidates in Eqs. (2).

Direct methods for solving first-kind equations (Eq. (3)) follow immediately from discretization of the integral. The direct midpoint-rule discretization of Eq. (2b) yields

$$f_1 = \frac{\left[\partial_t^{-1}R\right]_1}{\left[hK_H\left(\frac{h}{2}\right)\right]} \tag{5a}$$

$$f_n = \frac{1}{\left[hK_H\left(\frac{h}{2}\right)\right]}\left(\left[\partial_t^{-1}R\right]_n - h\sum_{i=1}^{n-1}K_{H,n-i}f_i\right), \tag{5b}$$

where

$$f_n = f_{\text{inc}}\left[\left(n - \tfrac{1}{2}\right)h\right] \tag{6a}$$

$$K_{H,n} = K_H\left[\left(n - \tfrac{1}{2}\right)h\right] \tag{6b}$$

$$\left[\partial_t^{-1}R\right]_n = \int_0^{nh} R(s)\,\mathrm{d}s \tag{6c}$$

are stepsize-h discretizations. Notice that if

$$\left|hK_H(h/2)\right| \ll \min\left(\left|f_n\right|, \left|\left[\partial_t^{-1}R\right]_n\right|\right) \tag{7}$$

then the parenthetical numerator of Eq. (5b) would be a small difference of large numbers, which would cause a loss of significant digits. Candidate (2b) is therefore preferred because a propagation-of-singularities argument [3] shows that $K_H(0^+) \neq 0$, whereas candidates Eqs. (2c), (2d), et seq. have integral kernels that are continuous and zero at $t = 0$, with the zeros being first order for K_{tH}, second order for K_{t^2H}, and so forth. Indeed, numerical experiments have shown that the above-described loss of significant digits causes a rapid numerical blowup for the first-order-zero case (Eq. (2c)). Thus, Eq. (2b) is the best of the infinitely many algorithms in Eqs. (2).

We turn now to the numerical properties of the best method, Eq. (2b).

Linz [2] has shown that error in the the direct midpoint-rule solution of first-kind Volterra equations is

$$f_{\text{exact}} - f_n = \frac{h^2}{24}\varepsilon_n + O(h^4), \tag{8}$$

where ε_n is independent of the stepsize h. Examining the algorithm (2b) in light of Eqs. (4) and (8), we see that smoothing the data reduces the algorithm's ill-posedness, and that the smoothed data $\partial_t^{-1} R$ are fed into an algorithm Eq. (5) that is stable and second-order accurate, and for which Richardson extrapolation [2], based on Eq. (8), would yield a fourth-order-accurate solution. For any given error criterion, the h^4 method would allow one to increase the stepsize and thereby further reduce the method's noise sensitivity according to Eq. (4).

An obvious challenge in using Eq. (2b) is the accommodation of the large amount of numerical noise that is caused by the FDTD propagation of the discontinuous function $\mathrm{H}(t)$ when computing K_{H}. The propagated discontinuity could have been avoided by instead propagating the ramp function $t\mathrm{H}(t)$ and then differentiating, as in $K_{\mathrm{H}} = \partial_t K_{t\mathrm{H}}$, but noise would then have been introduced by numerical differentiation. Therefore, for the sake of simplicity, the kernel K_{H} is computed directly by propagating $\mathrm{H}(t)$, which is similar to a process whose usefulness has already been established [4]. The stepsize h is decreased until the h-dependent, discontinuity-related noise is contained in a frequency band that is separated from the spectrum of the main physical features of K_{H}. In practice (Section 4) the numerical noise consisted of oscillations whose periods varied from $10h$ to $20h$, regardless of the value of h. A 40-point centered filter Φ was then defined, using $t_{\mathrm{m}} = 19h$ and $T_{\mathrm{M}} = 20h$ in (A1). The Appendix uses Φ to derive the identity

$$\partial_t^{-1}(\Phi * R) = (\Phi * K_{\mathrm{H}}) * f_{\mathrm{inc}}, \tag{9}$$

in which $*$ henceforth represents $\int_{-\infty}^{t}$-type convolution. Notice that both Eq. (9) and its unfiltered predecessor Eq. (2b) are exact for all t. The next, and final, numerical consideration will, however, lead to an approximate version of Eqs. (2b) and (9).

The wavefront of an FDTD-computed field travels with the superluminal velocity c/CFL because of the nature of time stepping in a CFL-stabilized computation. The filtered fields $(\Phi * R)$ and $(\Phi * K_{\mathrm{H}})$ were therefore truncated as

6

$$(\Phi * K_{\mathrm{H}}) \quad \overset{\mathcal{T}}{\longmapsto} \quad (\Phi * K_{\mathrm{H}})\,\mathrm{H}(t) \tag{10a}$$

$$(\Phi * R) \quad \overset{\mathcal{T}}{\longmapsto} \quad (\Phi * R)\,\mathrm{H}(t), \tag{10b}$$

where t is now measured with respect to the analytically determined wavefront-arrival time (t_{a}) at each receiver. (That arrival time is the same for all receivers in Figure 1. For more complicated media, the arrival time can be computed using characteristics or the eikonal equation [3].) The quantities on the right-hand sides of Eqs. (10a) and (10b) are used, respectively, as the K_{H} and R terms in Eq. (5). Notice that the truncation in Eq. (10a) of the necessarily superluminal FDTD-computed K_{H} assures that the right-hand side of Eq. (10a) will have an initial discontinuity, which is beneficial from the standpoint of Eq. (7). This may be the only known computational advantage of the superluminal feature of FDTD. If, however, K_{H} had been computed exactly by analytical means then, because of a propagation-of-singularities argument [3], it would already have been discontinuous and, because exact computations have no noise, filtering would not have been necessary. Regardless of whether K_{H} is computed exactly or with filtered-then-truncated FDTD, one does obtain a discontinuous integral kernel that, together with an exact or filtered-then-truncated R, can be fed into Eq. (5), with the same numerical benefits that Eqs. (4), (7), and (8) ordinarily yield.

The main disadvantage of truncation is that the procedure of feeding Eq. (10) into Eq. (5) is inherently approximate, unlike Eq. (9) which uses filtered-but-untruncated data. The Appendix shows that the truncation errors in (10), however, will vanish in the $h \to 0$ limit, provided that the underlying FDTD computation is reasonable; and in that matter there is a fine point Eq. (A16) that arises from a discontinuity.

This section has considered infinitely many — but not all — time-domain methods. Resolvent-kernel methods [10], for example, seem especially appealing for processing many received signals; for if one could solve $(\Phi * K_{\mathrm{H}}) * \rho = 1$ for ρ, then (filtered) incident fields could be quickly inferred using $\Phi * f = R * (\Phi * \rho) - R(0^{+})\partial_{t}^{-1}(\Phi * \rho)$. A numerical experiment, however, showed that solving $(\Phi * K_{\mathrm{H}}) * \rho = 1$ can be ill conditioned, but many other resolvent-kernel methods remain unexplored.

4. NUMERICAL SOLUTION

This report's prototype problem was defined in Figure 1 and Section 2. The incident field was a one-cycle 5.45-GHz sinusoidal pulse. That carrier frequency had been chosen to be at the midpoint of the operating band of the existing

antenna [5] that this problem models. The corresponding wavelength was 5.5 cm, which can be compared in Figure 1 with the 3-cm element ($\times$ symbol) spacing and the 6-cm disk diameter. The steel disk had a 10^7-S/m conductivity and its permittivity was that of free space, and the remainder of Figure 1 had free-space properties.

Fields were computed with an FDTD program that was written [6] in accordance with an early manuscript version of [7], and whose absorbing boundary condition was later replaced [6] with a Berenger PML [8]. This FDTD program is second-order accurate in space and time. The program was run with CFL $= 1/2$ and for several grid refinements. The discontinuity-related noise in the K_H computation decreased as the grid was refined, and the spectra of the noise and the main physical features of the computed signals were well separated on the finest spatial grid (2840×5232), which yielded 4735 points per carrier-frequency period. The same 2840×5232 grid was used to compute each one-cycle-sinusoid response $R_j(t)$ in Figure 2 and to compute K_H.
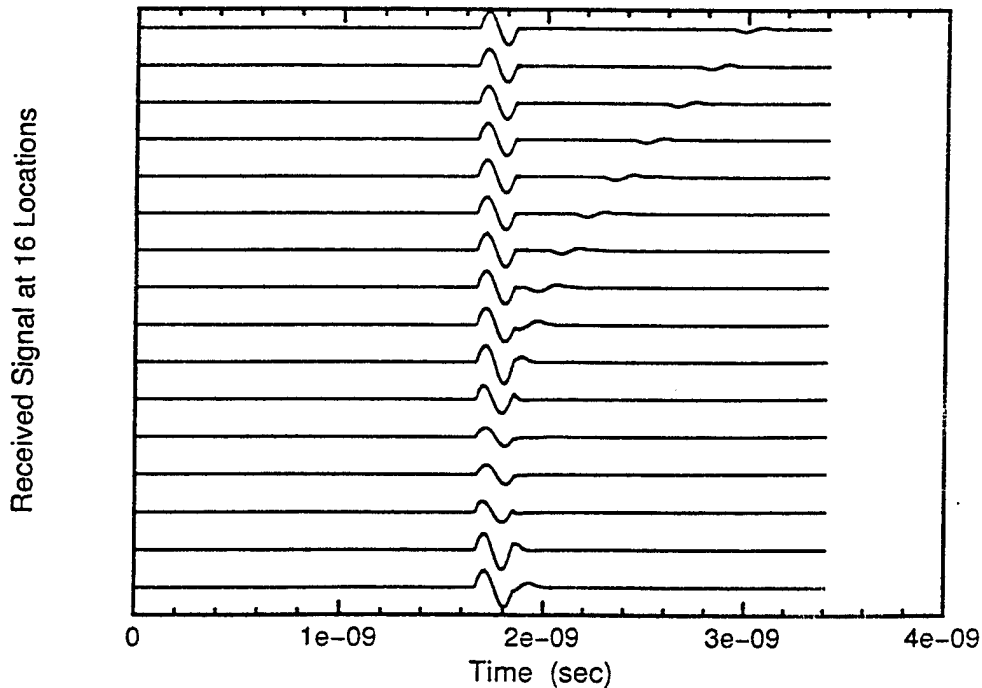

Figure 2. The total signal received at every other location in Figure 1. These 16 signals have different vertical offsets, with the largest and smallest offsets used, respectively, for the top and next-to-bottom $\times$-marked locations in Figure 1. Note the disk's shadow and the delayed-wave components.

8

The integral kernel K_H and each received signal R_j were both convolved with the 40-point filter Φ, as described in Eqs. (9) and (A1). The filtered functions $\Phi * R_j$ and $\Phi * K_H$ were truncated as in Eqs. (10) and (A7), and then the time origin was shifted so that $t = 0$ represented the pulses' analytically determined arrival times (t_a). The filtered, truncated, time-shifted pulses were fed into a second-order-accurate routine (Eq. (5)). Each received signal was deconvolved separately from the 31 other signals, resulting in 32 independent inferences of the incident field f_{inc}. A typical reconstruction is shown in Figure 3, which corresponds to the signal received at the 15th cross from the bottom of Figure 1. Figure 4 shows that each of the 32 second-order-accurate reconstructions of f_{inc} (dash-dotted curve with circles) reproduces the L_∞ norm of the one-cycle sinusoid (flat, boldfaced curve) f_{inc} within 2%. The L_2 norm (not graphed), whose square is proportional to the energy of a free-space pulse, is reproduced to within 1.3% error.
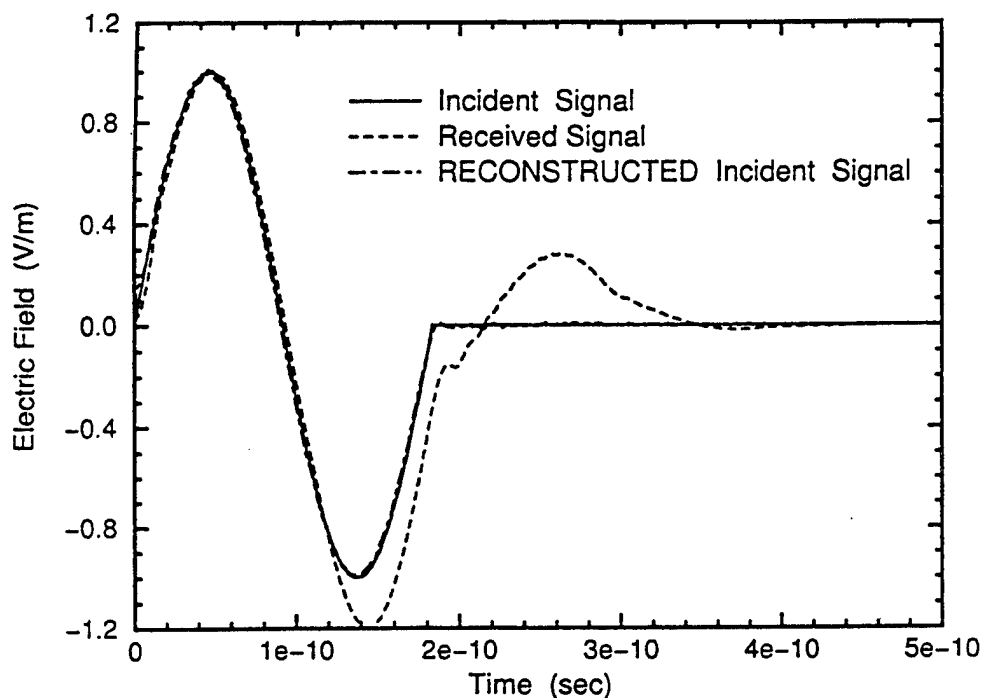

Figure 3. Reconstruction of the incident signal f_{inc}, using the signal received at the 15th location from the bottom of Figure 1. The incident signal and its reconstruction almost overlap.
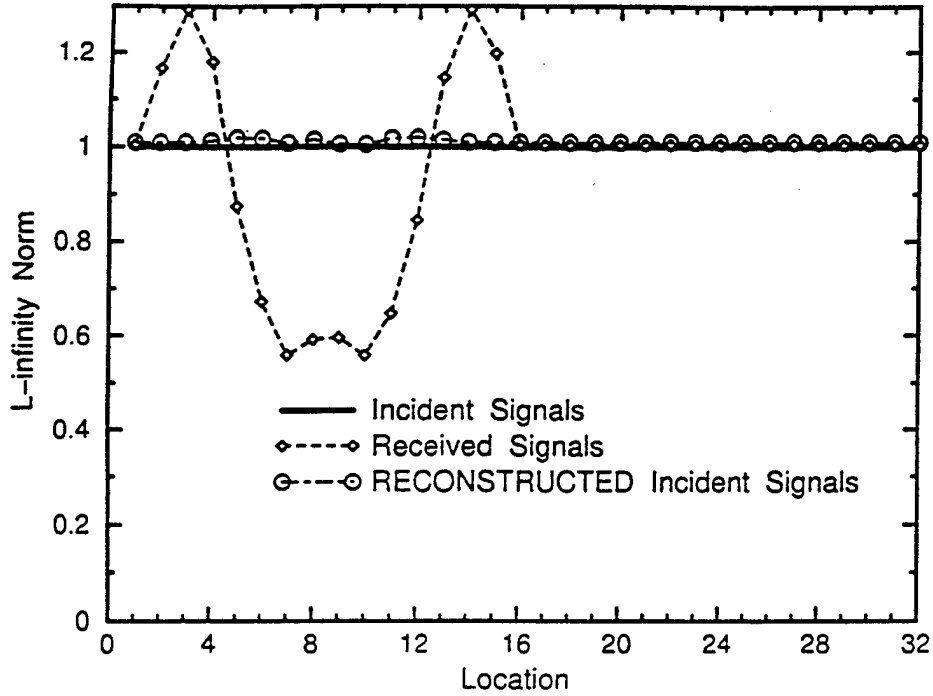
Figure 4. Restoration of the L_∞ norm for the 32 locations in Figure 1. Note the shadow and diffractive foci of the received signals. The reconstructed signals' norms were within 2% of $\|f_{\text{inc}}\|_{L_\infty}$, which was 1.

The predominant error in these $O(h^2)$ results is barely evident in Figures 3–4. To find the predominant reconstruction error in Figure 3, look along the left-hand vertical axis for a brief, diagonal segment near 0.15 V/m. Similar features in all 32 of the $O(h^2)$ reconstructions predominate the relative errors $\|f_{\text{reconstructed}} - f_{\text{inc}}\|/\|f_{\text{inc}}\|$ that are illustrated in Figure 5. Richardson extrapolation was used [2] to obtain the $O(h^4)$ results in Figure 5. We see there that the extrapolation reduced the L_∞ relative error from $\approx 11\%$ to $\approx 8\%$, but that the L_2 error remained $\approx 4\%$. A detailed inspection of each $O(h^4)$ time trace showed that it differed from the corresponding $O(h^2)$ graph mainly in the first extrapolated data point. It appears unlikely, however, that these small, brief reconstruction errors would have any practical significance for the radar problem that these computations model. That model radar problem, after all, has a steel pipe (Figure 1) that causes a deep shadow and diffractive foci in the received signals (Figure 4), which both the $O(h^2)$ and $O(h^4)$ deconvolutions have largely removed (Figures 3–5).
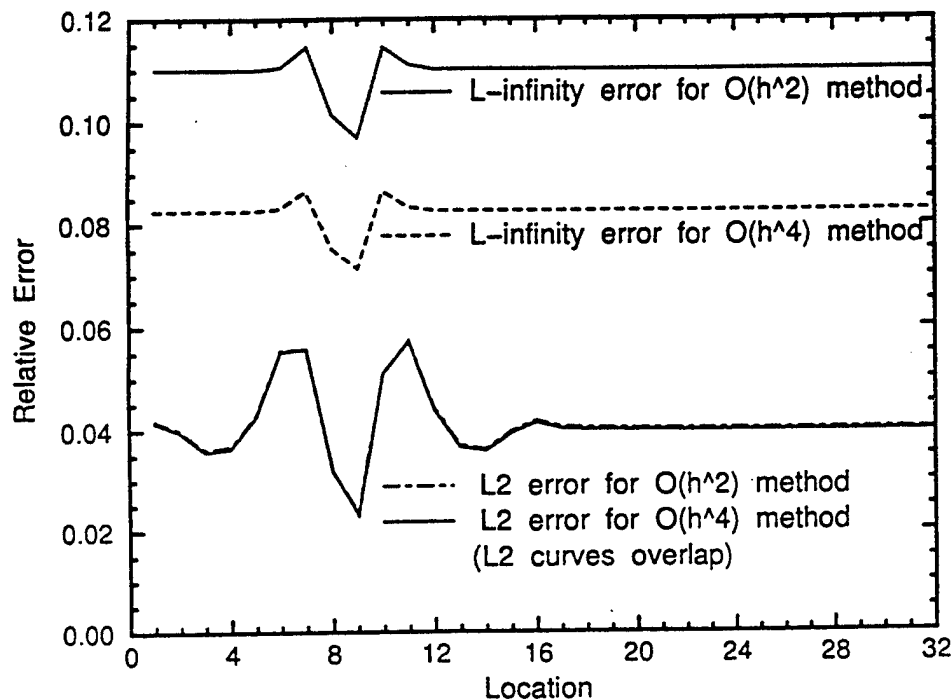
Figure 5. L_p relative errors in the reconstructed signals. Richardson extrapolation decreased the L_∞ error considerably, but left the L_2 error essentially unchanged.

5. CONCLUSION

This report is related to [4], which used FDTD to compute the Kronecker-delta-function response, K_δ, which [4] then used to propagate other incident fields f_{inc} using Eq. (2a). Reference [4] considered other reference pulses as alternatives to K_δ, but it concluded that K_δ was the simplest reference pulse to use. Thus, K_δ and Eq. (2a) are best for the (convolutional) forward-propagation problem of [4], and K_H and Eq. (2b) are best for the (deconvolutional) reconstruction problem in the present report. These two combined methods Eqs. (2a)–(2b) are useful despite their integral kernels being FDTD-computed responses to discontinuous fields. The t-domain-deconvolution method of Eq. (2b), for example, is stable and $O(h^2)$ accurate — it is $O(h^4)$ accurate after Richardson extrapolation — and it consequently may compete with frequency-domain methods.

11

Significant work was required because of the numerical error in a computed Heaviside response K_H. Because a discontinuous integral kernel tends to conserve significant digits, as shown by Eq. (7), it was best to truncate $(\mathcal{T})$ the FDTD-computed K_H and then filter out (Φ) the large-amplitude, high-frequency noise that would otherwise have obliterated the $\mathcal{T}$-restored discontinuity. Those steps would have been unnecessary were K_H known exactly.

We finally consider what one could do in practice, using laboratory data. Heaviside-step pulses are problematical in the laboratory, so it is likely that K_H would have to be inferred from other measurements. For removing interference in an operating band $[\omega_{\min}, \omega_{\text{MAX}}]$, for example, one could presumably infer K_H by propagating a reference pulse f_{ref} whose spectrum covers $[\omega_{\min}, \omega_{\text{MAX}}]$ and whose risetime is $\ll 2\pi/\omega$. To infer K_H one would then solve Eq. (2b) for K_H using the received signals R resulting from the known $f_{\text{inc}} = f_{\text{ref}}$. If such a K_H were truncated, then the result could presumably be used to reduce interference in the operating band $[\omega_{\min}, \omega_{\text{MAX}}]$. There are two final observations: The response to a short-risetime f_{ref} can be synthesized by superimposing the responses to several band-limited signals. Second, as long as the propagation remains linear, the techniques developed here apply regardless of whether multiple scattering is evident in that linear propagation.

This appendix derives the identities Eqs. (A4)–(A5), which are used in the development Eq. (9) of this report's numerical method. That numerical method also uses a truncation-related approximation that is studied here in Eqs. (A7)–(A16) and shown, under a reasonable assumption, to vanish as the stepsize h tends to 0. The assumption is that the superluminal parts of the FDTD-computed R and K_H tend to 0 pointwise as $h \to 0$.

The numerical example in Section 4 uses a centered filter

$$f \quad \xmapsto{\Phi} \quad \frac{1}{T_M + t_m} \int_{-t_m}^{T_M} f(t + s)\mathrm{d}s, \tag{A1}$$

for which t_m differs from T_M by at most one timestep (h), and $\min(t_m, T_M) > 0$. That filter is also a convolution on $(-\infty, \infty)$

$$\Phi * f = \int_{-\infty}^{\infty} \Phi(t - s)f(s)\mathrm{d}s \tag{A2}$$

$$\Phi(t) = (T_M + t_m)^{-1}\, \mathrm{H}(t + T_M)\mathrm{H}(t_m - t), \tag{A3}$$

for a generic function f. We also note that $f_{\mathrm{inc}}(t) = f_{\mathrm{inc}}(t)\mathrm{H}(t)$, $R(t) = R(t)\mathrm{H}(t - t_c)$, and $K_H(t) = K_H(t)\mathrm{H}(t - t_c)$, where $t_c = t_a\mathrm{CFL} < t_a$ is the (superluminal) FDTD-computed pulse-arrival time and t_a is the analytical (lightspeed) pulse-arrival time. We will assume that $t_c \geq T_M$, as is true for the computation in Section 4. Next we will show that

$$\Phi * \left(\partial_t^{-1} R\right) = \partial_t^{-1}\left(\Phi * R\right) \tag{A4}$$

$$\Phi * \left(K_H * f_{\mathrm{inc}}\right) = \left(\Phi * K_H\right) * f_{\mathrm{inc}} \tag{A5}$$

identically for all $t \in (-\infty, \infty)$.

To derive Eq. (A4), use Eq. (A1) and the obvious definition of the antiderivative ∂_t^{-1}, and use a change of variables, to establish

$$\partial_t^{-1}\left(\Phi * R\right) = \frac{1}{T_M + t_m} \int_{-t_m}^{T_M} \mathrm{d}s' \int_{s'}^{t+s'} \mathrm{d}s R(s), \tag{A6}$$

13

which is identifiable as Eq. (A4) because $T_M \leq t_c$ and $R(t) = R(t)H(t - t_c)$. Equation (A5) merely asserts the elementary associative property of convolution. The identities (Eqs. (2b) and (A4)–(A5)) yield Eq. (9).

Although Eqs. (A4)–(A5) are identities for any linear system, such as physical scattering or its FDTD approximation, the computations in Section 4 used truncated quantities

$$\mathcal{T} \circ f(t) = f(t)H(t - t_a) \tag{A7}$$

for $f \in \{K_H, R\}$ as in Eq. (10). Such truncation introduces errors

$$\Delta_R = \partial_t^{-1} \left[\mathcal{T} \circ (\Phi * R) \right] - \partial_t^{-1} (\Phi * R) \tag{A8}$$

$$\Delta_K = \left[\mathcal{T} \circ (\Phi * K_H) \right] * f_{inc} - (\Phi * K_H) * f_{inc} \tag{A9}$$

because the FDTD-computed functions K_H and R are supported on $[t_c, \infty]$ and because $t_c = t_a\mathrm{CFL} < t_a$. We will now estimate Δ_R and Δ_K, starting with Δ_R.

Equation (A1) implies

$$\Phi * f = (\Phi * f)H(t + T_M - t_c) \tag{A10}$$

for $f \in \{R, K_H\}$. Evaluate Eq. (A8) using Eqs. (A7) and (A10) to show that $\Delta_R = -\int_{t_c-T_M}^{t_a} (\Phi * R)\mathrm{d}s$, which is independent of t. Apply Eq. (A1) and a change of variables to the previous equation to establish

$$\Delta_R = \frac{-1}{T_M + t_m} \int_{-t_m}^{T_M} \int_{t_c-T_M+s'}^{t_a+s'} R(s)\mathrm{d}s\mathrm{d}s'. \tag{A11}$$

Use Eq. (A11) and the triangle inequality to estimate $|\Delta_R|$ by bringing the absolute value through the integrals, then integrating the result over the union of all s'-dependent intervals of integration in the inner integral of Eq. (A11), and then using $R(t) = R(t)H(t - t_c)$ to obtain

$$|\Delta_R| \leq \left\| R \right\|_{L_1(t_c, t_a+T_M)}. \tag{A12}$$

The previous norm is over an interval that is only slightly larger, by an amount T_M, than the support of the superluminal part of the FDTD-computed R. The assumption in this appendix's first paragraph and the observation that $T_M \to 0$ as $h \to 0$ (because $T_M = 20h$ in Section 4) then imply that $\Delta_R \to 0$ as $h \to 0$.

14

Now we estimate Δ_K in the $h \to 0$ limit. Use the Young theorem [9] and the identity $\mathcal{T} \circ (\Phi * K_H) = \mathrm{H}(t + T_M - t_c)\mathrm{H}(t - t_a)(\Phi * K_H)$ to evaluate Eq. (A9) and obtain

$$\left\| \Delta_K \right\|_{\mathrm{L}_s(-\infty, \infty)} \leq \left\| \Phi * K_H \right\|_{\mathrm{L}_\sigma[t_c - T_M, t_a]} \left\| f_{\mathrm{inc}} \right\|_{\mathrm{L}_p[0, t_a]} \tag{A13}$$

for all $s, p \in [1, \infty]$, where $\sigma^{-1} = 1 + s^{-1} - p^{-1}$. We will use Eq. (A13) to show $\lim_{h \to 0} \Delta_K = 0$ by establishing that there is a σ for which

$$\lim_{h \to 0} \left\| \Phi * K_H \right\|_{\mathrm{L}_\sigma[t_c - T_M, t_a]} = 0. \tag{A14}$$

Indeed, we will show that Eq. (A14) applies for all $\sigma \in [1, \infty)$, the exclusion of ∞ being notable. For $\sigma = \infty$ one can proceed in the most straightforward way, using Eq. (A1) and $K_H(t) = K_H(t)\mathrm{H}(t - t_c)$, to obtain

$$\left\| \Phi * K_H \right\|_{\mathrm{L}_\infty[a, b]} \leq \left\| K_H \right\|_{\mathrm{L}_\infty[a - t_m, b + T_M]}, \tag{A15}$$

for any $a \leq b$. The $\sigma = \infty$ case is excluded from Eq. (A14) because Eq. (A15) would bound the $\mathrm{L}_\infty[t_c - T_M, t_a]$ norm of $\Phi * K_H$ from above by the $\mathrm{L}_\infty[t_c, t_a + T_M]$ norm of K_H, which cannot be forced to 0 as $h \to 0$ because of the h-independent discontinuity at $t = t_a$ of the exact, analytical K_H; but Eq. (A15) will soon be used as a lemma. Because K_H is discontinuous at $t = t_a$, we now evaluate the $\mathrm{L}_\sigma(t_c - T_M, t_a)$ norm $(\sigma < \infty)$ of $\Phi * K_H$ by estimating separately the $\int_{t_c - T_M}^{t_a - T_M}$ and $\int_{t_a - T_M}^{t_a}$ components of the definition of that L_σ norm. The result, after some straightforward manipulation involving Eq. (A15), is

$$\left\| \Phi * K_H \right\|_{\mathrm{L}_\sigma[t_c - T_M, t_a]}^\sigma \leq (t_a - t_c) \left\| K_H \right\|_{\mathrm{L}_\infty[t_c, t_a]}^\sigma + T_M \left\| K_H \right\|_{\mathrm{L}_\infty[t_a - T_M - t_m, t_a + T_M]}^\sigma \tag{A16}$$

for all $\sigma \in [1, \infty)$. The first term in the sum in Eq. (A16) vanishes as $h \to 0$ because of the assumption in this appendix's first paragraph. Then $\lim_{h \to 0} T_M = 0$ implies that the left-hand side of Eq. (A16) vanishes in the same limit; and $\Delta_K \to 0$, too, because of Eq. (A13). We have now shown, subject to the assumption at the beginning of this paragraph, that $\max(|\Delta_R|, |\Delta_K|) \to 0$ as $h \to 0$. Thus, the error introduced by truncation in Eqs. (10) and (A7)–(A9) vanishes as $h \to 0$, provided the underlying FDTD method is reasonable, as defined in the first paragraph of this Appendix.

REFERENCES AND NOTES

[1] Steyskal, H. (1994) Synthesis of antenna patterns with imposed near-field nulls, *Electronics Letters* **30**, 2000–2001.

[2] Linz, Peter (1985) *Analytical and Numerical Methods for Volterra Equations* SIAM, Philadelphia, Pennsylvania, Chapter 9.

[3] Courant, R. and Hilbert, D. (1962) *Methods of Mathematical Physics* Volume II, Interscience, New York, pages 115–118, 416–421, 512–515, and 620–635.

[4] Kriegsman, Gregory A. and Luke, Jonathan H. C. (1994), Rapid pulse responses for scattering problems, *J. Comput. Phys.* **111**, 390–398.

[5] Eber, Louis (1988) Digital Beam Steering Antenna, Technical Report RADC-TR-88-83, U.S. Air Force, Attachment 2, ADA200030.

[6] Petropoulos, Peter G. (1997) Department of Mathematics, Southern Methodist University, Dallas, Texas 75275 (personal communication).

[7] Taflove, Allen (1995) *Computational Electrodynamics: the Finite-difference Time-domain Method* Artech House, Boston.

[8] Berenger, Jean-Pierre (1994) A perfectly matched layer for the absorption of electromagnetic waves, *J. Comput. Physics* **114**, 185-200.

[9] Reed, Michael and Simon, Barry (1975) *Methods of Modern Mathematical Physics* Volume II, Academic Press, New York, pages 29 and 32.

[10] Gripenberg, Gustaf (1980) On Volterra Equations of the First Kind, *Integral Equations and Operator Theory* **3**, 473–488.